EXTENDED EXPERIMENTAL PROCEDURES

Cell Culture

We obtained HEK293T cells and 3T3-L1 cells from ATCC (CRL-11268 and CL-173). Human mesenchymal cells were generated from H9 embryonic stem cells (WiCell) and isolated by anti-CD73 FACS (BD PharMingen, 550257) as previously described (Woo et al., 2010). Cells were grown under sterile, humidified conditions (37°C, 5% CO_2) in DMEM/10% FCS (HEK293T and 3T3-L1 cells) or in Mesenchymal Stem Cell-GM BulletKit (Lonza, PT-3001). We regularly screened for and excluded infections, including Mycoplasma contamination (Maxim Biotech).

Cloning, Transduction, and Cell Treatment

We cloned a single moiety of the ubiquitin gene (NP_061828) and of PPARγ isoform 1 (NP_619725) into pRetroX-IRES-ZsGreen1 (Clontech) with an N-terminal 3FLAG tag (Sigma Aldrich). ChIP recovery with 3FLAG-ubiquitin was superior to anti-ubiquitin antibodies or other tags we tested (data not shown) (Zhang et al., 2008). The constructs for PSMB1 (NP_002784), c-Jun (NP_002219), and NCoR1 (NP_001239242) were cloned with an N-terminal 3FLAG tag and an IRES-GFP construct into pLVX-tight-puro (Clontech) and cells were transduced in the presence of a tetracycline repressor (Clontech). CREB (NP_598589) was cloned with an N-terminal HA tag into pcDNA3.1 (Invitrogen). The KID mutation was performed by removing positions 99-149 of the CREB protein sequence. The RID mutation of NCoR1 is lacking amino acids C-terminal of position 1,917. The human *NDUFV1* promoter was obtained as a Renilla construct (SwitchGear Genomics) and the CRE (TGACGTCT) upstream of the TSS was removed in the (ΔCRE) mutant. Infections were performed with VSV-G serotyped virus, produced by HEK293T cells. All transduced cells were sorted to > 95% purity based on green fluorescence. Knockdown of NCoR1, Siah2, and CREB in 3T3-L1 cells was achieved with specific shRNA (pLKO, Open Biosystems) and selected with puromycin. Double knockdown was performed by first selecting with one construct and then infecting with an MOI of 10 for the second construct. Changing the sequence of transduction yielded similar results (data not shown). Scrambled shRNA (pLKO) was used as a negative control (Open Biosystems). Lactacystin (Boston Biochem) was dissolved in DMSO and applied at 0.1% vol/vol (25 μM) for three or six hours or as indicated. The same concentration and solvent was used for forskolin (Cayman Chemical) and FCCP (Carbonyl cyanide 4-(trifluoro-methoxy)phenyl-hydrazone; Sigma-Aldrich). All cells that are labeled as ''untreated'' received 0.1% vol/vol DMSO for the same duration as drugs were applied.

ChIP, ChIP-on-Chip, and ChIP Sequencing

ChIPs were performed with M2 (Sigma Aldrich), anti-RNA polymerase II (Millipore, 05-623), anti-CREB (Millipore, 17-600 and Cell Signaling Technology, #9197), anti-Phospho-CREB (Millipore, 17-10131), anti-H3K27ac (Millipore, 17-683), and anti-H3K4me3 (Abcam, ab1012) antibodies at 4 μg/reaction per 10^7 cells. Sequential ChIPs for ubiquitinated NCoR1 were performed with a poly-ubiquitin binding resin (Boston Biochem, S5α peptide agarose) under low salt conditions (25 mM NaCl). For sequential ChIPs with endogenous NCoR1 and CREB, the first round eluate was obtained by heating to 75°C and in the absence of any detergent. H3K4me3 data were used to standardize the correlation to highly expressed genes (data not shown). ChIP was performed on Triton X-100 isolated nuclei. We fixed cells in 1% para-Formaldehyde (in PBS) at 37°C for 10 min. Sonication was performed with a Branson Digital Sonifier (Tip 102C) for ChIP-on-chip and ChIP-qPCR experiments and with a Covaris S2 sonicator (AFA fiber microtubes, 6x16 mm) for ChIP-seq. For ChIP-on-chip, material was hybridized with Nimblegen's 385k RefSeq Promoter arrays (hg18) at Nimblegen's core facility (Reykjavik, Iceland). DNA was amplified using the WGA2 and WGA3 kit (Sigma Aldrich). 12 ChIP-seq experiments were performed with 3T3-L1 cells including one total genomic DNA control run. DNA was prepared according to Illumina's protocols for single-end sequencing (HiSeq 2000). The average alignment score to the mm9 genome was 88.2% with $201x10^6$ aligned reads. As reference for ChIP-qPCR, we used 1%–10% of total DNA. On a technical note, the recovery of DNA linked to the proteasome subunit PSMB1 was several orders of magnitude lower than the yield with ubiquitin. ChIP-seq peaks, lists of annotated target genes, and ChIP-on-chip results are included in the Table S1.

Immunoblots and Coimmunoprecipitations

Immunoblots were performed on 4%–12% SDS-PAGE gradient gels (Invitrogen) under reducing conditions (10 mM DTT). Lysate was generated by boiling in 1% SDS. Semi-dry hybridization (Bio-Rad) was performed on PVDF (Invitrogen). Lysate was normalized by cell count and by protein concentration (10 μg per lane). Antibodies for the following antigens were used: CREB (Cell Signaling Technology, clone 48H2), S5α (Cell Signaling Technology, #3846), H3-HRP (Abcam, ab21054), GAPDH-HRP (Cell Signaling Technology, #3683), Siah2 (Abcam, ab72064), NCoR1 (Millipore, 17-10260), and HA (Cell Signaling Technology, #3724). Co-IPs of proteasome subunits were performed in Triton X-100 lysed cytosol, Co-IPs for NCoR1 were conducted in isolated, sonicated nuclei. IP/Westerns were performed without cross-linking.

Gene Expression Analyses

Whole-genome expression arrays in human mesenchymal cells were performed on Nimblegen's 385k expression arrays (Keck Microarray Resource, Yale University) and on Affymetrix Mouse Gene 1.0 ST arrays for 3T3-L1 cells (Partners Center for Personalized Genetic Medicine). Libraries were constructed using oligo-dT in combination with random hexamer priming. SYBR-Green based

RT-qPCR (Invitrogen) was performed with transcript-specific reverse transcription. Amplicons were verified by melting curve or gel electrophoresis. Gene expression values are listed in Table S2.

Use of Public Records

Chromatin states in 3T3-L1 cells are based on GSE20752 (Mikkelsen et al., 2010). Whole-genome expression values of HEK293T cells were obtained from entry GSM711410 (Takahashi et al., 2011). ChIP-seq data on NCoR1 is based on ERR103444 (Raghav et al., 2012). FASTQ files were converted with the FASTQ Groomer (https://main.g2.bx.psu.edu/) (Blankenberg et al., 2010; Giardine et al., 2005; Goecks et al., 2010), mapped with Bowtie and converted with SAM-to-BAM prior to standard peak calling (see below).

Data Processing and Statistics

Libraries were prepared according to Illumina's instructions (New England Biolabs, Cat. No. E6200). Briefly, DNA was end-repaired using a combination of T4 DNA polymerase, *E. coli* DNA Pol I large fragment (Klenow polymerase) and T4 polynucleotide kinase. The blunt, phosphorylated ends were treated with Klenow fragment (32 to 52 exo minus) and dATP to yield a protruding 3- 'A' base for ligation of Illumina's adapters which have a single 'T' base overhang at the 3′ end. After adaptor ligation DNA was PCR amplified with Illumina primers for 15 cycles and library fragments of ~250 bp (insert plus adaptor and PCR primer sequences) were band isolated from an agarose gel. The purified DNA was captured on an Illumina flow cell for cluster generation. Libraries were sequenced on the Genome Analyzer following the manufacturer's protocols. Sequence reads were obtained and mapped to the mouse mm9 genome using the Illumina Genome Analyzer Pipeline. The bigwigs were created with the following steps: Reads were aligned to the reference genome using bowtie with at most 2 mismatches. The SAM file with those alignments was converted to BAM format and then sorted using samtools, and then the sorted alignments were converted to wig format using a custom python script. Finally, the wigs were converted to bigWigs using wigToBigWig (which can be downloaded from http://hgdownload.cse.ucsc.edu/admin/exe/). Annotations are based on the mm9 genome build. ChIP-sequencing peaks were called with MACS1.4 (www.cistrome.org) (Feng et al., 2012; Liu et al., 2011). Motif detection was performed with the SeqPos module with a window of 2 kbp. GO analyses were conducted with DAVID (http://david.abcc.ncifcrf.gov/) (Huang da et al., 2009). We calculated regional overlaps with BEDTools (Quinlan and Hall, 2010) and used random genomic regions of equal size on the same chromosomes as reference. Relative enrichment was calculated based on overlap with these random sites and 10 randomizations were performed to obtain arithmetic mean and standard deviation. To ensure compatibility of our peak calling algorithm with the published chromatin states, we used MACS1.4 on a test-set of entry GSE20752 and identified > 80% regional overlap with the published peaks (data not shown). We also found strong correlation with previously published binding patterns of PPARγ, validating the use of the 3FLAG tag as well as the compatibility between data processing pipelines (data not shown). Based on GSE20752, chromatin marks H3K27me3 and H3K36me3 constitute the prevalent epigenomic modifications (35.7% and 33.5% of the genome) (data not shown). Statistical tests were calculated as indicated with STATA (Release 12). Unless indicated otherwise, all tests are based on the Two-sided Wilcoxon rank-sum test with Bonferroni correction. The TATA box was defined as such and the relative occurrence of this tetrameric sequence was calculated based on a region spanning 100 bp upstream of 25,499 transcription start sites.

Immunohistochemistry

Immunohistochemistry was conducted with the M2-Cy3 antibody (Sigma Aldrich) after fixing in 4% p-FA and permeabilization with 0.1% Triton X-100. Epifluorescent pictures were obtained on a Nikon Eclipse TE2000-U (200x magnification). Nuclei were counterstained with DAPI.

Electrophysiological Experiments

For quantification of mitochondrial membrane potential, we labeled cells with 350 pM DiOC6(3) (3,3-Dihexyloxacarbocyanine iodide, Sigma Aldrich) for 30 min at 37°C, 5% CO_2 in DMEM/10% FCS, then washed with PBS and immediately analyzed by FACS. Confocal microscopy of JC-1 stained cells was performed with a Nikon Eclipse Ti. JC-1 (5′,6,6′-tetrachloro-1,1′,3,3′-tetraethyl-benzimidazolylcarbocyanine iodide, Cayman Chemical) was applied for 15 min at 10 μM. Mitochondria were quantified with Mitotracker and FACS (15 min, 100 nM MitoTracker Red-CMXRos, Invitrogen) or by qPCR of genomic mouse DNA. Experiments were performed with triplicate samples and independently confirmed.

Primers

Mouse genomic primers:

Actin B Fwd: AAGTGCCTGACTCCATGAGAA
Actin B Rev: GCAAGAAGATGCCTCCAGAT
mtCOX1 Fwd: CAGACCGCAACCTAAACACA
mtCOX1 Rev: GGTGCCCAAAGAATCAGAAC
AKAP1 Fwd: AGGTTACGGGAAAGCCAGAT
AKAP1 Rev: GGGTTCCTGGTGTCTGAGTG
MRPS18b Fwd: TGTTGCTGAGGCTTGTTTGT

MRPS18b Rev: TTAAAGGCGACCCGTACTGA
NDUFV1 Fwd: CAGGACGATTCCGCTGTAGT
NDUFV1 Rev: GTAGTCCAGCTTGCCCAGAC
Albumin Fwd: ACTCCAGACCCGTTTCACAC
Albumin Rev: GGAGGGGTGGGTCTCATTAT

Mouse and other expression primers, based on PrimerBank (Wang and Seed, 2003):

GAPDH Fwd: AGGTCGGTGTGAACGGATTTG
GAPDH Rev: GGGGTCGTTGATGGCAACA
HSPA8 Fwd: TCTCGGCACCACCTACTCC
HSPA8 Rev: CCCGATCAGACGTTTGGCA
AKAP1 Fwd: ATGGCAATCCAGTTGCGTTC
AKAP1 Rev: TCCACCTGCTTATCACTGCTG
MRPS18b Fwd: TTGCGGCACACGCTTCTAAA
MRPS18b Rev: CTTCCAAGGCTCGCTCTCAT
NDUFV1 Fwd: GTGCGGGTATCTGTGCGTT
NDUFV1 Rev: GGTTGGTAAAGATCCGGTCTTC
Renilla Fwd: GGTCAGAAGACCAACCCTCA
Renilla Rev: CACGATAGCGTTGCTGAAGA

SUPPLEMENTAL REFERENCES

Blankenberg, D., Von Kuster, G., Coraor, N., Ananda, G., Lazarus, R., Mangan, M., Nekrutenko, A., and Taylor, J. (2010). Galaxy: a web-based genome analysis tool for experimentalists. Curr. Protoc. Mol. Biol. *89*, 10.1–10.21.

Feng, J., Liu, T., Qin, B., Zhang, Y., and Liu, X.S. (2012). Identifying ChIP-seq enrichment using MACS. Nat. Protoc. *7*, 1728–1740.

Giardine, B., Riemer, C., Hardison, R.C., Burhans, R., Elnitski, L., Shah, P., Zhang, Y., Blankenberg, D., Albert, I., Taylor, J., et al. (2005). Galaxy: a platform for interactive large-scale genome analysis. Genome Res. *15*, 1451–1455.

Goecks, J., Nekrutenko, A., and Taylor, J.; Galaxy Team (2010). Galaxy: a comprehensive approach for supporting accessible, reproducible, and transparent computational research in the life sciences. Genome Biol. *11*, R86.

Impey, S., McCorkle, S.R., Cha-Molstad, H., Dwyer, J.M., Yochum, G.S., Boss, J.M., McWeeney, S., Dunn, J.J., Mandel, G., and Goodman, R.H. (2004). Defining the CREB regulon: a genome-wide analysis of transcription factor regulatory regions. Cell *119*, 1041–1054.

Liu, T., Ortiz, J.A., Taing, L., Meyer, C.A., Lee, B., Zhang, Y., Shin, H., Wong, S.S., Ma, J., Lei, Y., et al. (2011). Cistrome: an integrative platform for transcriptional regulation studies. Genome Biol. *12*, R83.

Nielsen, R., Pedersen, T.A., Hagenbeek, D., Moulos, P., Siersbaek, R., Megens, E., Denissov, S., Børgesen, M., Francoijs, K.J., Mandrup, S., and Stunnenberg, H.G. (2008). Genome-wide profiling of PPARgamma:RXR and RNA polymerase II occupancy reveals temporal activation of distinct metabolic pathways and changes in RXR dimer composition during adipogenesis. Genes Dev. *22*, 2953–2967.

Quinlan, A.R., and Hall, I.M. (2010). BEDTools: a flexible suite of utilities for comparing genomic features. Bioinformatics *26*, 841–842.

Ratner, J.N., Balasubramanian, B., Corden, J., Warren, S.L., and Bregman, D.B. (1998). Ultraviolet radiation-induced ubiquitination and proteasomal degradation of the large subunit of RNA polymerase II. Implications for transcription-coupled DNA repair. J. Biol. Chem. *273*, 5184–5189.

Takahashi, H., Parmely, T.J., Sato, S., Tomomori-Sato, C., Banks, C.A., Kong, S.E., Szutorisz, H., Swanson, S.K., Martin-Brown, S., Washburn, M.P., et al. (2011). Human mediator subunit MED26 functions as a docking site for transcription elongation factors. Cell *146*, 92–104.

Wang, X., and Seed, B. (2003). A PCR primer bank for quantitative gene expression analysis. Nucleic Acids Res. *31*, e154.

Wang, L., Xu, S., Lee, J.E., Baldridge, A., Grullon, S., Peng, W., and Ge, K. (2013). Histone H3K9 methyltransferase G9a represses PPARγ expression and adipogenesis. EMBO J. *32*, 45–59.

Woo, C.J., Kharchenko, P.V., Daheron, L., Park, P.J., and Kingston, R.E. (2010). A region of the human HOXD cluster that confers polycomb-group responsiveness. Cell *140*, 99–110.

Zhang, X., Odom, D.T., Koo, S.H., Conkright, M.D., Canettieri, G., Best, J., Chen, H., Jenner, R., Herbolsheimer, E., Jacobsen, E., et al. (2005). Genome-wide analysis of cAMP-response element binding protein occupancy, phosphorylation, and target gene activation in human tissues. Proc. Natl. Acad. Sci. USA *102*, 4459–4464.

Zhang, X., Guo, C., Chen, Y., Shulha, H.P., Schnetz, M.P., LaFramboise, T., Bartels, C.F., Markowitz, S., Weng, Z., Scacheri, P.C., and Wang, Z. (2008). Epitope tagging of endogenous proteins for genome-wide ChIP-chip studies. Nat. Methods *5*, 163–165.

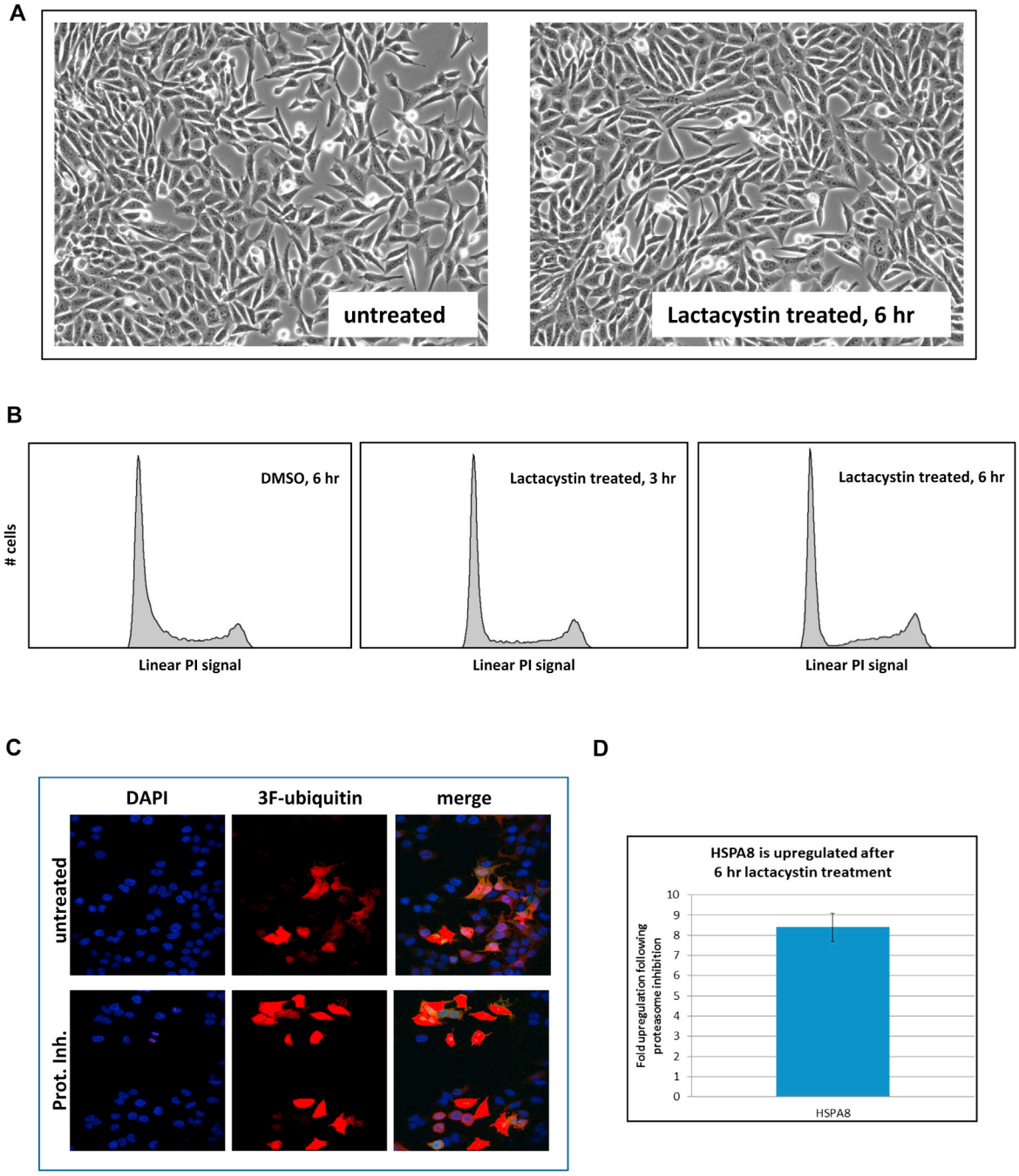

Figure S1. Short Proteasome Inhibition Does Not Perturb the Cellular Phenotype, Related to Figure 1

(A) 3T3-L1 cells were cultured in the presence of 0.1% DMSO or lactacystin (25 μM) for up to six hours without visible change in phenotype (Brightfield microscopy, 200x, Nikon Eclipse TE2000-U).

(B) Cell cycle distribution of 3T3-L1 cells only changes minimally following up to 6 hr of lactacystin treatment with G1 remaining the largest fraction (43.3%–50.1%). Cell cycle stages were examined by FACS following propidium-iodide staining and analyzed by the Watson Pragmatic algorithm.

(C) Immunohistochemistry of 3FLAG-ubiquitin transduced 3T3-L1 cells after treatment with lactacystin (6 hr). Proteasome inhibition does not alter the cellular distribution of ubiquitin.

(D) To confirm proteasome inhibition, we examined cells for increased expression of the heat shock protein HSPA8 by RT-qPCR after lactacystin treatment (6 hr). Bars represent mean ± SD.

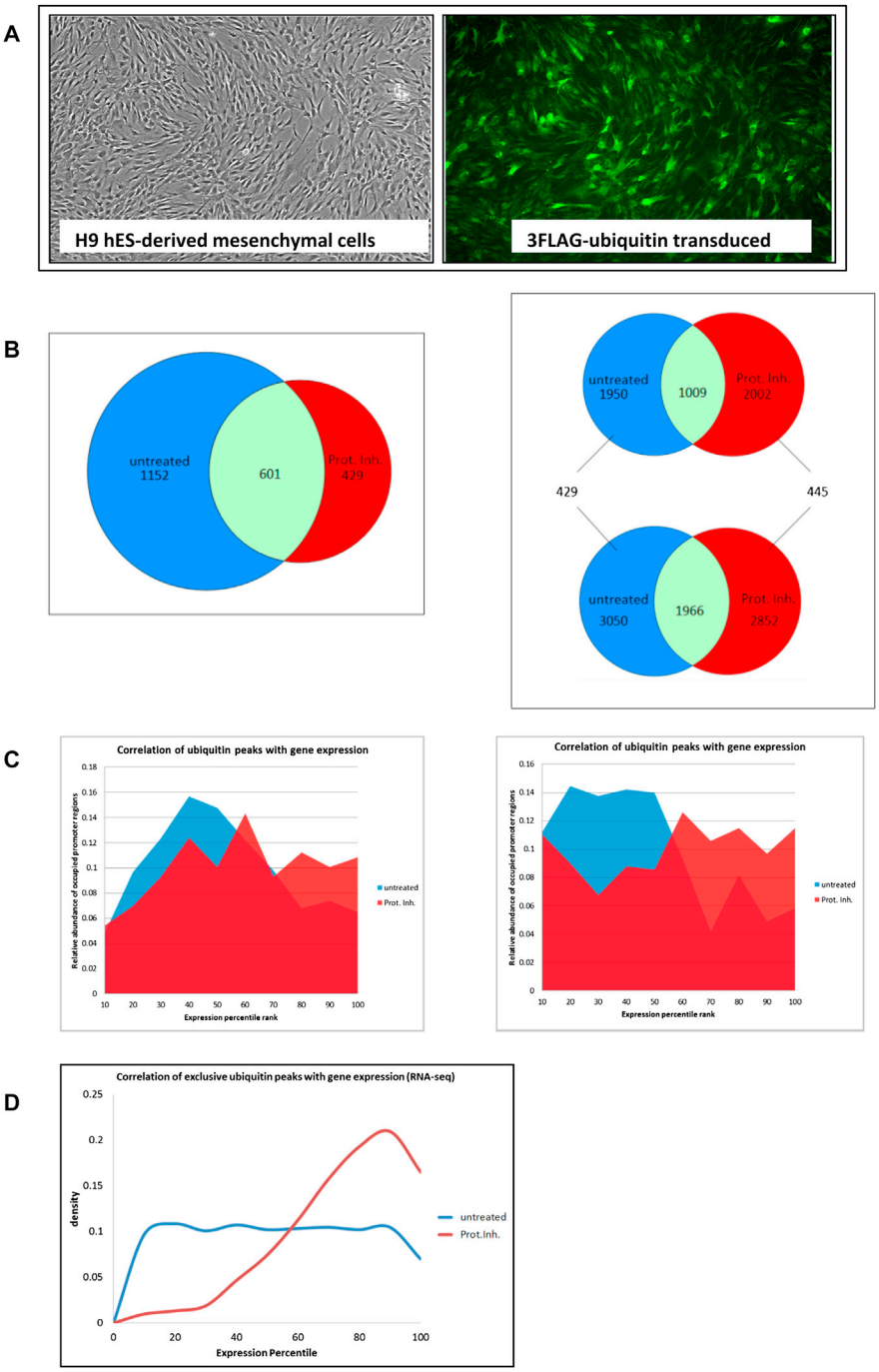

Figure S2. ChIP-on-Chip Pilot Experiments Using Human Promoter Arrays, Related to Figure 2

(A) Mesenchymal cells were differentiated from human H9 ES cells and isolated based on CD73 surface expression. After transduction with 3FLAG-ubiquitin, cells were selected using IRES-driven expression of a green fluorescent marker protein.

(B) One ChIP-on-chip experiment was performed with 3FLAG-ubiquitin transduced HEK293T cells (left panel) and two independent experiments were performed with 3FLAG-ubiquitin transduced H9-derived mesenchymal cells (right panel). In H9-derived cells, 445 and 429 genes were reproducibly and uniquely enriched for ubiquitination in the treated (25 μM lactacystin for 3 hr) or untreated sample.

(C) 1,152 steady state ubiquitin peaks and 429 degradation-prone ubiquitin peaks for HEK293T cells (left panel) and 429 and 445 peaks for H9-derived cells (right panel) were correlated based on expression values. Proteolysis is significantly enriched at the promoters of highly expressed genes ($p = 0.000878$ for HEK293T cells and $p = 3.2 \times 10^{-08}$ for H9-derived cells).

(D) Representation of unique ubiquitin peaks as in Figure 2B. Gene expression levels are based on RNA-sequencing (Wang et al., 2013) as opposed to microarrays in Figures 2A and 2B.

A

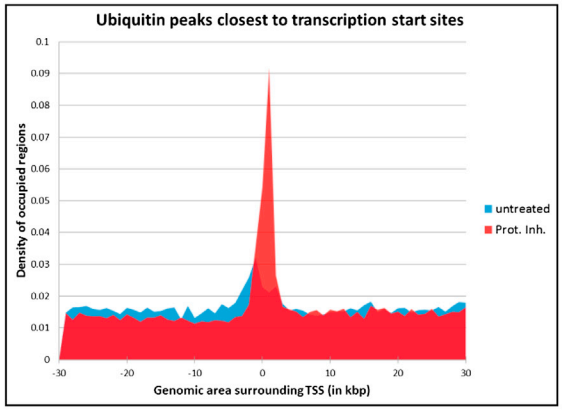

B

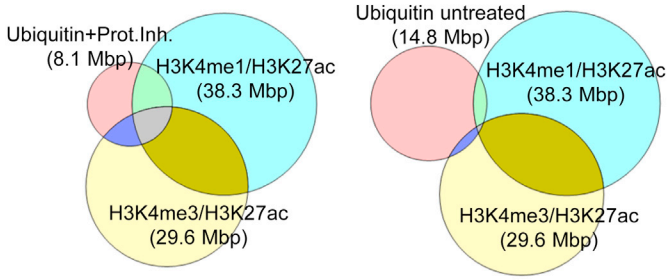

C

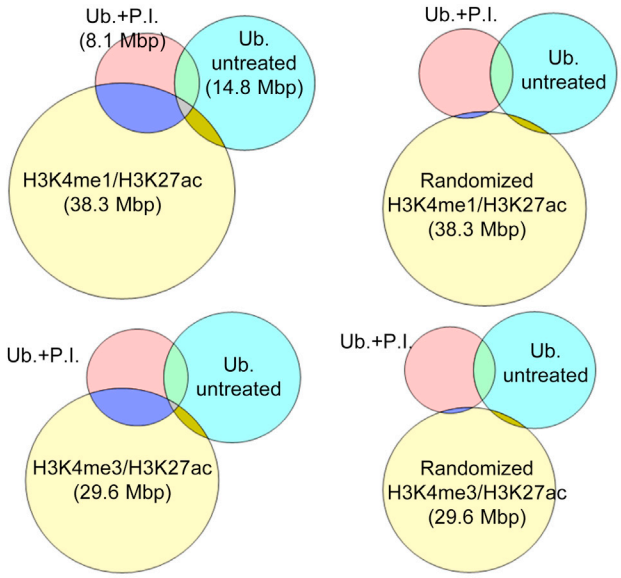

D

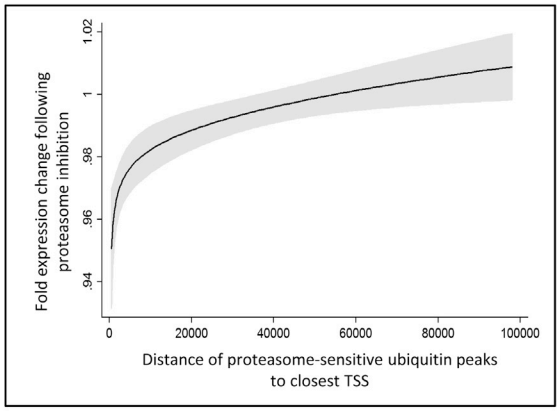

E

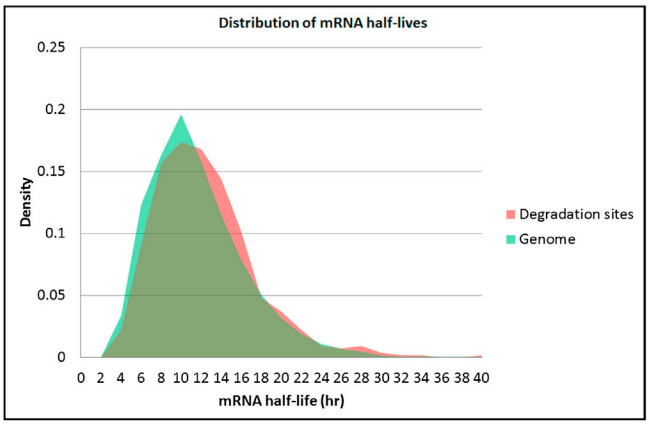

F

GO terms	p-values
Transcription factor activity	1.3E-8
Pattern specification	1.3E-5
Mitochondrion	3.3E-3
Plasma membrane	3.7E-3

G

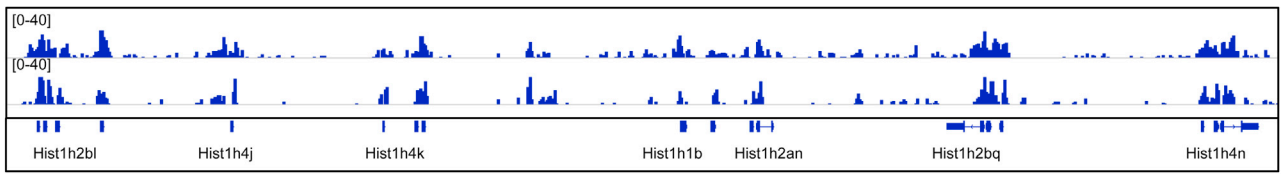

(legend on next page)

Figure S3. Analysis of Genomic Ubiquitin Distribution, Related to Figures 2 and 3

(A) Ubiquitin peaks in relation to transcription start sites (TSS). Degradative ubiquitination is more strongly associated with the TSS compared to steady state ubiquitination. Plot is not quantitative for overall binding pattern or strength but specifically counts only the peaks closest to the proximal TSS.

(B) Size of ubiquitin peaks (in Mbp) and putative active enhancers (H3K4me1/H3K27ac) and promoters (H3K4me3/H3K27ac) and their overlaps (left panels).

(C) Enhancer and promoter regions of equal size were randomly generated with the same chromosomal distribution with BEDTools to estimate non-specific overlaps (right panels).

(D) Expression changes of genes following lactacystin treatment (6 hr, y axis), compared to the distance of the closest degradation site (in bp, x axis). Overall, there is a trend for suppression of genes with degradation close to the TSS. 7,236 ubiquitin peaks (after 3 hr treatment) were considered with up to 100 kbp distance from the closest TSS. Expression values were listed based on distance in bins of 50 and 144 medians were collected. The plot represents a fractional polynomial regression of these median values with 95% confidence interval (gray shade).

(E) The half-lives of mRNA of genes with TSS within 3 kbp of degradation peaks do not significantly differ from the average mRNA half-life. Data are based on Schwanhäusser et al. (2011).

(F) Gene ontologies associated with degradative ubiquitination based on ChIP-on-chip with H9-derived human mesenchymal progenitor cells.

(G) Profiles of ubiquitin peaks in lactacystin-treated cells correlate with the position of promoters within the mouse major histone cluster. Shown are ChIP-seq tracks of two independent experiments (chromosome 13, position 21,800,000 to 21,940,000).

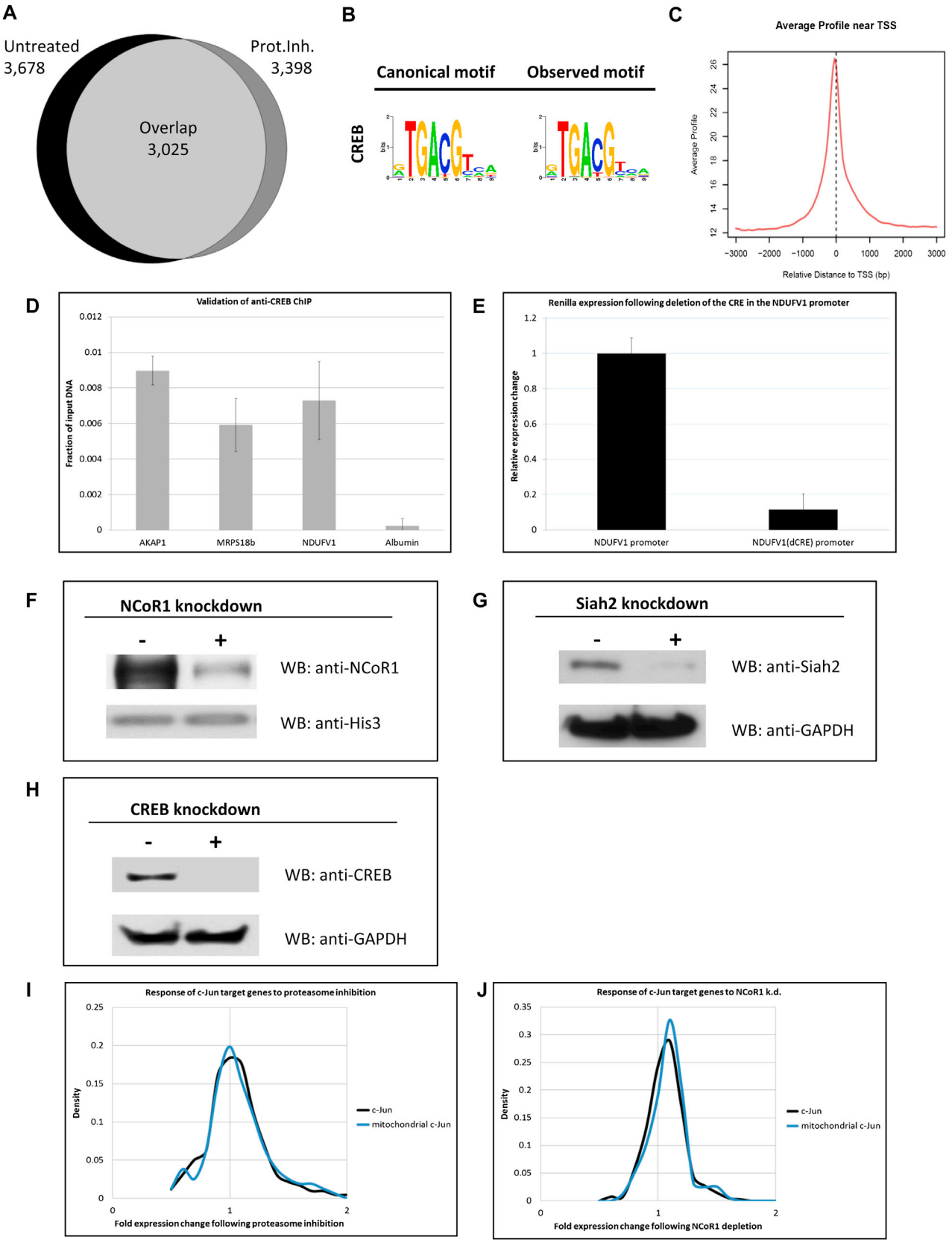

(legend on next page)

Figure S4. Quality Control of CREB Binding Data and of Knockdown Efficiencies, Related to Figures 4 and 5

(A) ChIP-seq experiments with CREB. Shown is a Venn diagram with the numbers of genes that have CREB binding sites within 3 kbp of TSS. Lactacystin treatment (3 hr) has no major influence on overall CREB distribution. We assigned the same target genes in 89.02% (including the three mitochondrial genes *AKAP1*, *MRPS18b*, and *NDUFV1*). The number and quality of genes was comparable to previous findings (Impey et al., 2004; Zhang et al., 2005). Peaks were visually inspected and showed a narrow distribution.

(B) A series of validations was performed to assess the quality of the ChIP-seq experiments. Motif analysis confirmed the CREB motif as the highest ranking binding site ($p < 10^{-157}$).

(C) Functional CRE motifs are found mostly within 250 bp of the TSS (Impey et al., 2004; Zhang et al., 2005). Our data confirmed that CREB binds predominantly within 1 kbp of the TSS.

(D) Assigned CREB genes were sensitive to treatment with the cAMP amplifying drug forskolin. In agreement with previous reports, this response was modest on a genome-wide scale (Altarejos and Montminy, 2011; Conkright et al., 2003) but still significant (not shown; $p = 1.33 \times 10^{-10}$). CREB genes were particularly sensitive (i.e., upregulated) to knockdown of CREB (not shown; $p = 9.42 \times 10^{-24}$). We performed confirming ChIP-qPCR with two different antibodies (Cell Signaling and Millipore) and had similar results. Shown is ChIP with the Millipore antibody that was also used for ChIP-seq).

(E) Deletion of the conserved CRE in the human *NDUFV1* promoter reduced expression of a Renilla construct 8-fold by RT-qPCR (GAPDH as reference), presumably due to the inability of CREB – or any other CRE-binding transcription factor – to bind to the promoter. Shown is data based on transfected HEK293T cells ($p < 0.01$, Two-sided Student's t-Test).

(F) Knockdown efficiency in 3T3-L1 cells for NCoR1 was assessed by IB of nuclear lysate with total Histone 3 as reference.

(G) Siah2 knockdown was confirmed on cell lysate with GAPDH as reference.

(H) As in panel B, shown is the knockdown efficiency for CREB. All three proteins were reduced > 75% by densitometry.

(I and J) (I) Mitochondrial target genes of c-Jun (based on ChIP-seq) were neither sensitive to lactacystin nor NCoR1 knockdown (J). Bars represent mean ± SD.

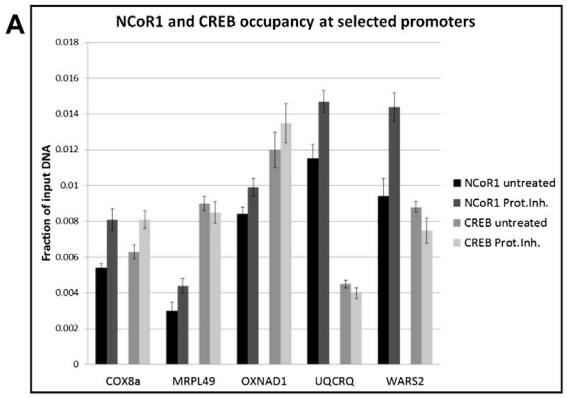

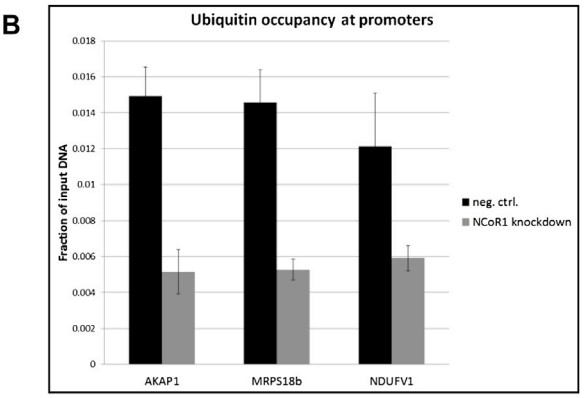

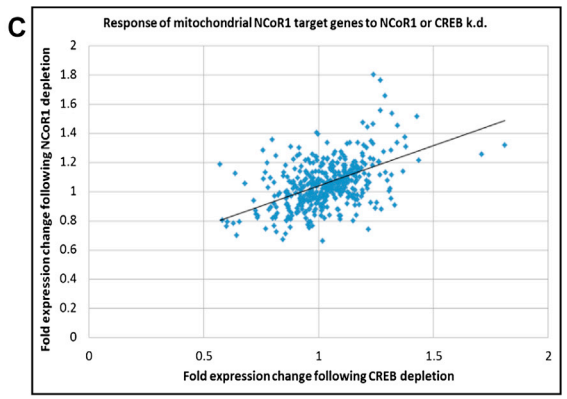

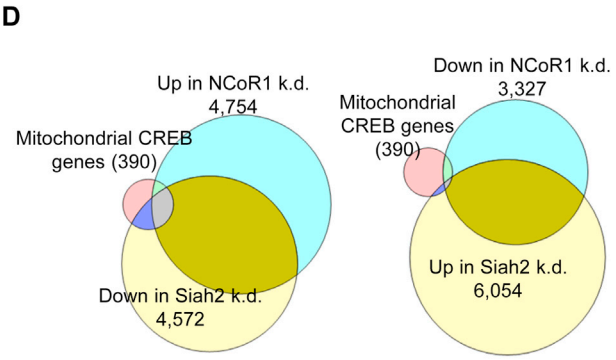

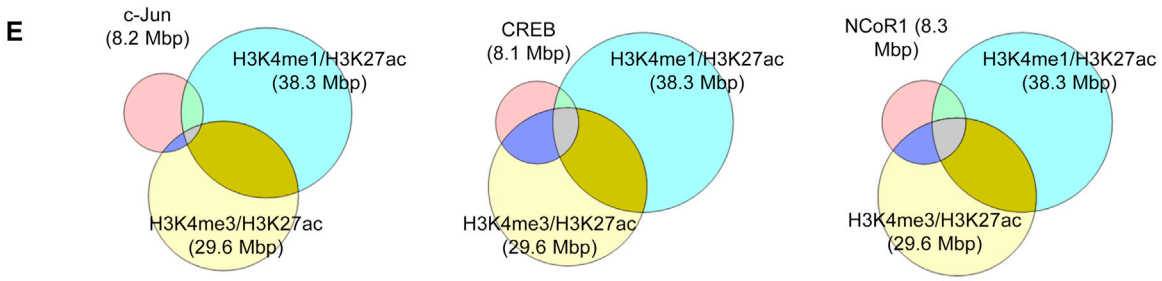

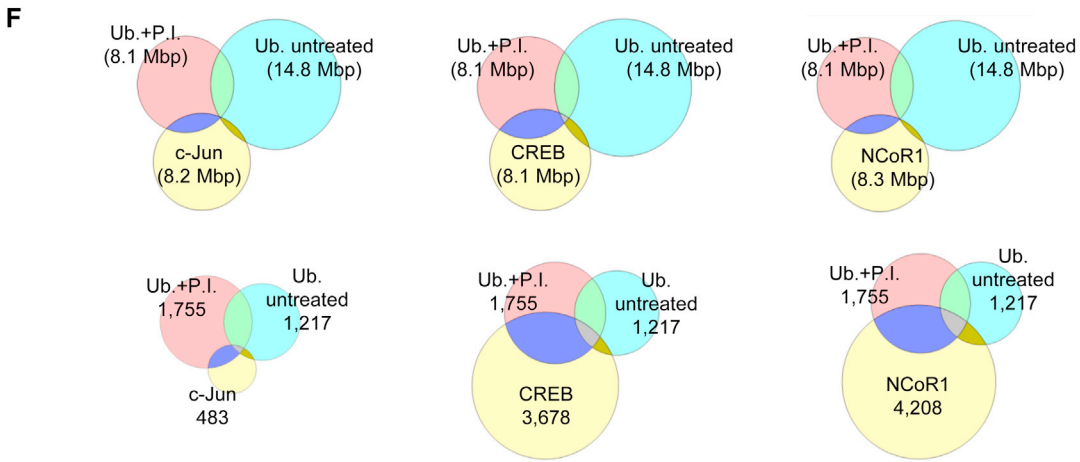

(legend on next page)

Figure S5. Comparison of DNA Binding between CREB and NCoR1, Related to Figure 5

(A) ChIP-qPCR of CREB and 3FLAG-NCoR1 in 3T3-L1 cells at promoters of nuclear encoded mitochondrial genes that are repressed by proteasome inhibition. Unlike CREB binding, NCoR1 occupancy consistently increases upon lactacystin treatment (3 hr).

(B) ChIP-qPCR with 3FLAG-ubiquitin in 3T3-L1 cells shows reduced promoter occupancy at the genes *AKAP1*, *MRPS18b*, and *NDUFV1* following NCoR1 knockdown ($p < 0.023$).

(C) High positive correlation in mitochondrial gene expression between NCoR1 and CREB depletion (correlation coefficient $\rho = 0.4673$).

(D) The Venn diagram shows overlaps between genes downregulated by NCoR1 and upregulated by Siah2 knockdowns. Expression changes were considered significant when being at least 10% altered (correlating approximately to being above the 80^{th} or below the 20^{th} percentile).

(E) Regional peak overlaps (in Mbp) between the three transcriptional regulators c-Jun, CREB, and NCoR1 and active enhancers and promoters.

(F) Regional peak overlaps (top panel) and overlaps based on assigned genes (TSS within 3 kbp of peak, bottom panel) between c-Jun, CREB, and NCoR1 and degradative (with proteasome inhibitor) or steady state ubiquitin (untreated). Bars represent mean ± SD.

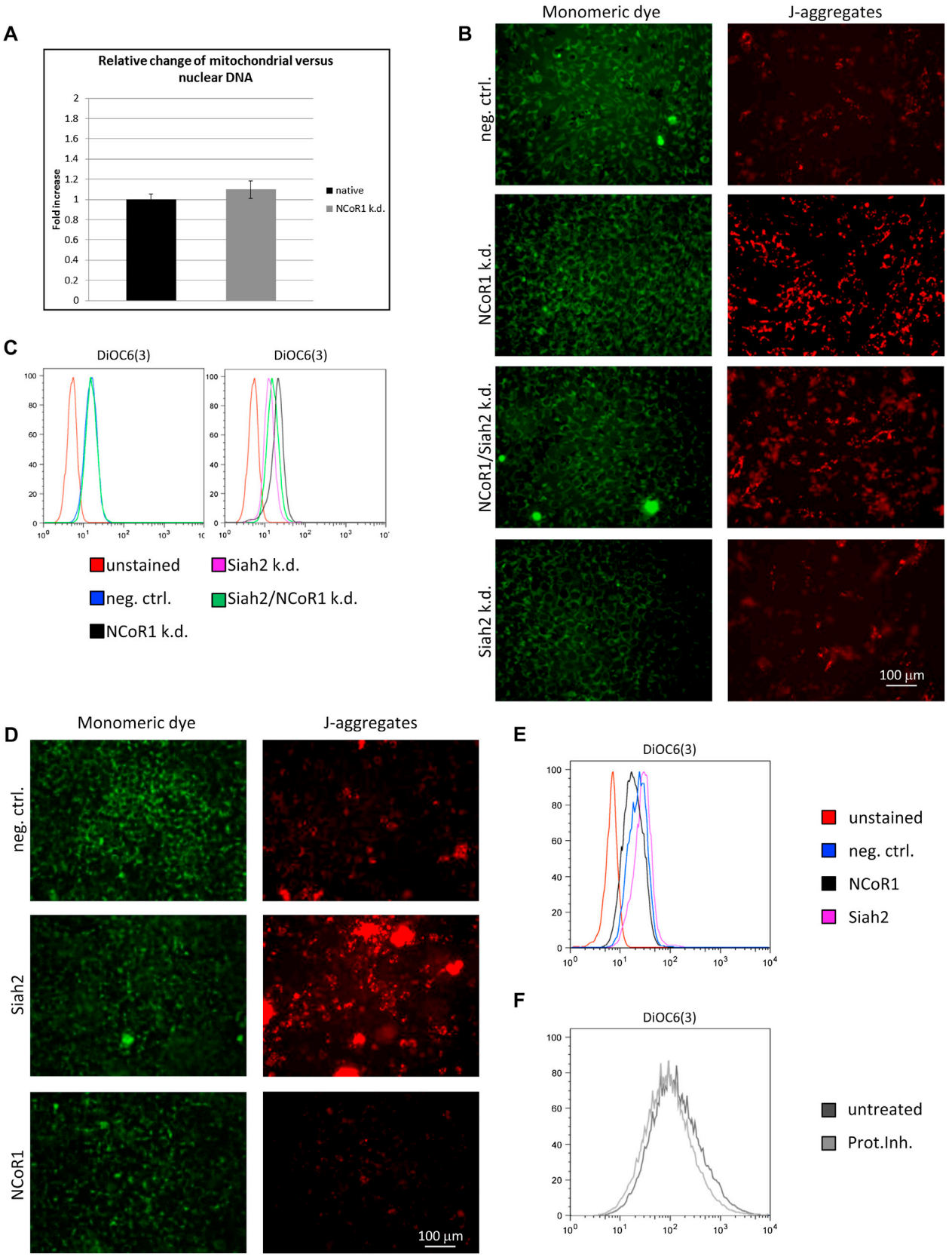

(legend on next page)

Figure S6. NCoR1 Effect on Mitochondria Physiology, Related to Figure 6

(A) Knockdown of NCoR1 does not affect the abundance of mitochondrial DNA. qPCR was performed for the mitochondrial gene COX1 with nuclear Actin B as reference.

(B) Labeling of 3T3-L1 cells as in Figure 6B. In addition, the effect of Siah2 knockdown alone is shown. We could not detect further reduction of J-aggregate formation.

(C) DiOC6(3) staining, however, was significantly reduced in Siah2 knockdown cells ($p < 0.05$).

(D and E) JC-1 and DiOC6(3) labeling of HEK293T cells 48 hr after transfection with empty vector control (blue), with NCoR1 (black), or Siah2 (purple) driven by a CMV promoter. Mean fluorescence intensity was significantly reduced by overexpression of NCoR1 and increased by overexpression of Siah2 ($p = 0.04$, Two-sided Student's t test).

(F) DiOC6(3) staining of 3T3-L1 cells after 18 hr of treatment with DMSO (dark gray) or 250 nM lactacystin (light gray). Gates were set for live cells, especially for panels E (Siah2 overexpression) and F. Bars represent mean ± SD.

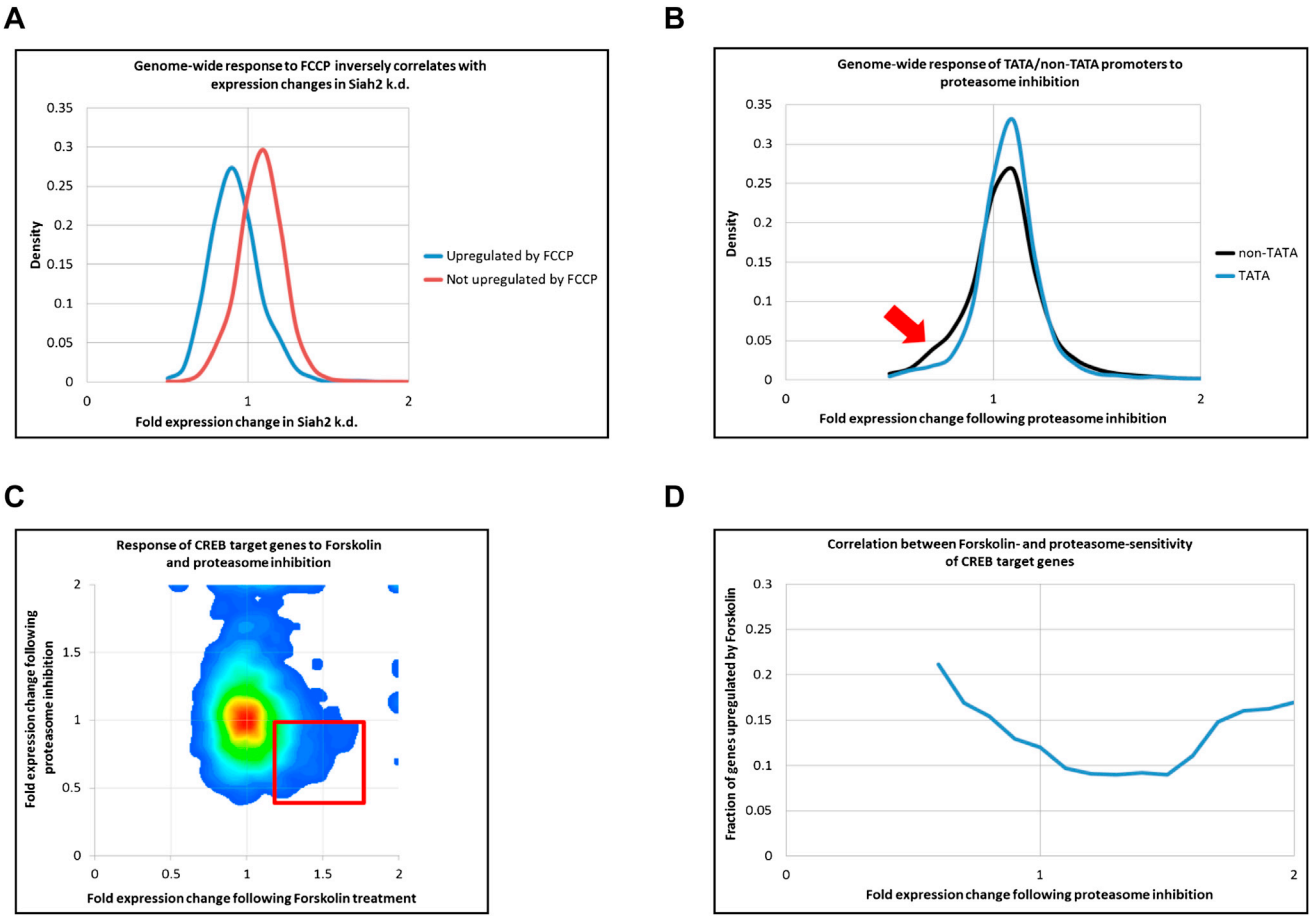

Figure S7. Gene Expression Changes following Mitochondrial and CREB Activation, Related to Figure 7

(A) Genes that were induced by FCCP (>1.2 fold, 6 hr treatment) were significantly repressed in Siah2 knockdown cells ($p < 4.51 \times 10^{-308}$).

(B) CREB target promoters are predominantly TATA-less in the human genome (Conkright et al., 2003). We reviewed our data and found comparable associations in mouse cells. The TATA box was underrepresented at CREB target genes (14.7% genome-wide versus 7.2% at CREB-bound promoters, $p = 1.21 \times 10^{-31}$, Two-sided Fisher's Exact Test). Moreover, TATA box containing genes were generally not repressed by proteasome inhibition (red arrow), indicating a fundamentally different mode of transcriptional control compared to the mostly non-TATA box containing CREB-bound promoters discussed in our study.

(C and D) Transcription response of 3,678 CREB target genes to forskolin treatment and proteasome inhibition (6 hr). Genes that were repressed by lactacystin were significantly induced by forskolin (red gate; $p = 0.0338$, Wilcoxon rank-sum test with Bonferroni correction).